Received: 23 April 2020 | Revised: 31 July 2020 | Accepted: 1 September 2020

DOI: 10.1096/fj.202000995R

RESEARCH ARTICLE

THE FASEB JOURNAL

Absence of uncoupling protein 3 at thermoneutrality influences brown adipose tissue mitochondrial functionality in mice

Elena Silvestri[1] | Rosalba Senese[2] | Rita De Matteis[3] | Federica Cioffi[1] | Maria Moreno[1] | Antonia Lanni[2] | Alessandra Gentile[4] | Rosa Anna Busiello[4] | Anna Maria Salzano[5] | Andrea Scaloni[5] | Pieter de Lange[2] | Fernando Goglia[1] | Assunta Lombardi[4]

[1]Department of Science and Technology, University of Sannio, Benevento, Italy

[2]Department of Environmental, Biological, and Pharmaceutical Sciences and Technologies, University of Campania "Luigi Vanvitelli", Caserta, Italy

[3]Department of Biomolecular Sciences, University of Urbino "Carlo Bo", Urbino, Italy

[4]Department of Biology, University of Naples Federico II, Naples, Italy

[5]Proteomics & Mass Spectrometry Laboratory, ISPAAM, National Research Council, Naples, Italy

Correspondence
Assunta Lombardi, Department of Biology, University of Naples Federico II, Complesso Universitario Monte Sant'Angelo, Edificio 7, Naples 80126, Italy.
Email: assunta.lombardi@unina.it

Fernando Goglia, Department of Science and Technologies, University of Sannio, via De Sanctis, Benevento 82100, Italy.

Abstract

The physiological role played by uncoupling protein 3 (UCP3) in brown adipose tissue (BAT) has not been fully elucidated so far. In the present study, we evaluated the impact of the absence of UCP3 on BAT mitochondrial functionality and morphology. To this purpose, wild type (WT) and UCP3 Knockout (KO) female mice were housed at thermoneutrality (30°C), a condition in which BAT contributes to energy homeostasis independently of its cold-induced thermogenic function. BAT mitochondria from UCP3 KO mice presented a lower ability to oxidize the fatty acids and glycerol-3-phosphate, and an enhanced oxidative stress as revealed by enhanced mitochondrial electron leak, lipid hydroperoxide levels, and induction of antioxidant mitochondrial enzymatic capacity. The absence of UCP3 also influenced the mitochondrial super-molecular protein aggregation, an important feature for fatty acid oxidation rate as well as for adequate cristae organization and mitochondrial shape. Indeed, electron microscopy revealed alterations in mitochondrial morphology in brown adipocytes from KO mice. In the whole, data here reported show that the absence of UCP3 results in a significant alteration of BAT mitochondrial physiology and morphology. These observations could also help to clarify some aspects of the association between metabolic disorders associated with low UCP3 levels, as previously reported in human studies.

Abbreviations: 8-OHdG, 8-hydroxy-2′-deoxyguanosine; ANT-1, adenine nucleotide transferase; BAT, brown adipose tissue; BN-PAGE, blue native polyacrylamide gel electrophoresis; CAT, catalase; CIII-UQCRC2, respiratory complex III (cytochrome b-c1 complex) subunit 2; CII-SDHB, respiratory complex II (succinate dehydrogenase) subunit B; CI-NDUF88, respiratory complex I (NADH:ubiquinone oxidoreductase) subunit NDUFB8; CIV-MTCO1, respiratory complex IV (cytochrome c oxidase) subunit 1; CV-ATP VA, complex V (ATP synthase) subunit VA; DIAPIT, protein upregulated during muscle growth 5 protein; FCCP, carbonylcyanide p-triflouromethoxyphenylhydrazone; FFAs, free fatty acids; G3P, glycerol 3-phosphate; GDP, guanosine diphosphate; GXP4, glutathione peroxidase 4; iBAT, intrascapular BAT; KO, UCP3 knockout mice; LD, lipid droplets; mG3PDH, mitochondrial glycerol-3-phosphate dehydrogenase; MITOS, mitochondrial inner membrane complex involved in maintenance of cristae junctions, inner membrane architecture and formation of contact sites to the outer membrane; nanoLC-ESI-LIT-MS/MS, nano-liquid chromatography-electrospray ionization-linear ion trap-tandem mass spectrometry; NTB, nitroblue tetrazolium; PAL-CAR, palmitoyl-carnitine; PLIN-1, perilipin-1; ROS, reactive oxygen species; SOD-2, superoxide dismutase 2; TEM, trasmission electron microscopy; UCP1, uncoupling protein 1; UCP3, uncoupling protein 3; VDAC, voltage-dependent anion-selective channel; WT, wild type.

Elena Silvestri and Rosalba Senese are contributed equally to this work.

Email: goglia@unisannio.it

Funding information
This study was funded by University of Sannio Research Grants, University of Urbino Grants and by the Department of Biology University of Naples Federico II (Ricerca di Base)

KEYWORDS
metabolism, oxidative stress, respiratory chain

1 | INTRODUCTION

Brown adipose tissue (BAT) is a thermogenic tissue able to convert the chemical energy into heat by consuming fatty acids. BAT mitochondria contain a relevant amount of uncoupling protein 1 (UCP1), which accounts for about 10% of their proteins. UCP1 is localized in the mitochondrial inner membrane and plays a pivotal role in the above-mentioned conversion.[1] By catalyzing proton leak under free fatty acid (FFA) activation, UCP1 allows the release of the energy contained in the mitochondrial electrochemical gradient in the form of heat. When UCP1 is active, substrate oxidation rates in BAT are very high, fulfilling the essential role of this tissue in thermoregulation, and sustaining its long-lasting thermogenic function. In some conditions (eg, cold exposure), in addition to using stored fats as substrates, BAT requires additional energy supplies such as serum glucose and lipids, thus improving the glucose metabolism and lipid profiles in certain conditions.[2] In adult humans, the amount of detectable BAT tissue inversely correlates with body mass index (BMI) and fat mass, and positively correlates with the resting metabolic rate (RMR).[3] Consequently, BAT is emerging as an effective new target to counteract some metabolic disorders such as, among others, the metabolic syndrome.[4,5] Moreover, BAT is less active under conditions of thermoneutrality, when only basal cellular reactions occur.[6] Nevertheless, BAT does still play a role in energy homeostasis at thermoneutrality, since under these conditions the absence of UCP1 induces obesity,[6] and alterations in BAT mitochondrial functionality affect the whole organism's metabolic fitness.[7] Exploiting this non-thermogenic function of BAT may offer novel means to contrast metabolic disorders, and studies on factors/proteins able to influence BAT mitochondrial functionality would be crucial to reach this goal. In this context, investigations performed on animal models maintained at thermoneutrality are better translatable to humans, in which only a modest basal activation of BAT occurs as result of their high body weight/surface area ratio and their predominant exposure to thermoneutral comfort zone.[8]

Besides UCP1, BAT contains uncoupling protein 3 (UCP3),[9,10] which is also present in other metabolically active tissues, such as skeletal muscle and heart.[11] The possible role of UCP3 in thermogenesis was initially discarded because, unlike UCP1-null mice, animals lacking UCP3 were able to adapt to an acute cold stimulus.[12,13] Moreover, Mills and coworkers demonstrated that UCP3-null mice display strongly blunted peak thermogenic and lethal responses to treatments with sympathomimetic drugs able to induce hyperthermia, such as 3,4-methylenedioxymethamphetamine and methamphetamine.[14-17] These mice also showed a completely abrogated lipopolysaccharide-induced thermogenesis.[16] In addition, Nau and coworkers reported data on a colony of Djungarian hamsters harboring a BAT selective loss of UCP3 expression (but normal UCP1) with a reduced cold tolerance, pointing to a role for this protein in maintaining BAT functionality.[18] Furthermore, UCP3 has been reported to be implicated in myocardial vulnerability to ischemia/reperfusion injury,[19-21] in metabolic homeostasis and in preventing some dysmetabolic diseases (obesity and insulin resistance).[22-24]

At the functional level, UCP3 mediates inducible proton leak, which is acutely activated only in the presence of some specific cofactors, including reactive oxygen species (ROS), FFAs, and fatty acid hydroperoxides.[10,25-27] To date, UCP3 has been shown to have key regulatory roles in fatty acid oxidation[28,29] as well as in preventing ROS- and lipid hydroperoxide-induced damages.[26,27]

Most of the studies on the impact of the absence of UCP3 on mitochondrial functionality have been focused on skeletal muscle and heart tissues. Attention has been given also to the role for UCP3 in BAT, despite the fact that this tissue contains a 10-fold higher amount of UCP3 protein with respect to muscle and heart.[10,30] Thus, revealing the role played by UCP3 in BAT is particularly intriguing, since in brown adipocytes this protein coexists together with UCP1, the universally accepted thermogenic protein. In view of the recent evidences in mice describing the role of UCP3 in energy and lipid metabolism also at thermoneutrality,[29] and of BAT impact on energy homeostasis also at thermoneutrality, we considered important to investigate the function played by UCP3 in "non-thermogenic" BAT physiology.

We evaluated the influence of the absence of UCP3 on BAT mitochondrial functionality in wild type (WT) and whole body UCP3-null (KO) mice housed at thermoneutrality. We focused our attention on: (a) BAT mitochondrial respiratory

parameters; (b) ROS production and antioxidant defenses; and (c) respiratory supercomplexes assembly and activities as well as mitochondrial and whole tissue morphology.

The analysis was limited to female animals only, knowing that a sexual dimorphism for adipose tissue physiology exists,[31] with implications for sex differences in relation to pathological conditions among which obesity. Female rodents, with respect to males, were suggested to have a greater energy expenditure (likely due to higher thermogenic activation) and a greater mitochondrial oxidative and respiratory/phosphorylative capacity.[32,33] Specifically in BAT, female rodents show higher expression levels of a number of genes involved in fatty acid oxidation and thermogenic regulation, and show a greater degree of metabolic adaptation in conditions of altered thermogenesis, such as caloric restriction.[34] Based on these considerations, the response of mitochondrial functionality in BAT of WT and KO female mice appeared interesting, as would be future studies on gender differences.

2 | MATERIALS AND METHODS

2.1 | Animals

Whole body UCP3-ablated Swiss Black mice (KO) were originally derived from Dr Reitman's lab.[13] KO and WT female mice (Swiss Black, Taconic, New York, USA) were housed at 30 ± 1°C, with a 12/12 hours light-dark cycle, and free access to food and water. After weaning, the animals were acclimated to thermoneutrality for 4 weeks. In order to test the morphological variations induced by acclimation of mice at thermoneutrality, a group of animals for each genotype was acclimated at 22 ± 1°C, for 4 weeks. At the end of the acclimation period, mice were anesthetized with pentothal (40 mg/100 g bw) and killed by decapitation. Blood and interscapular BAT (iBAT) were immediately collected and processed, or frozen in liquid nitrogen for later processing.

This study was carried out in accordance with recommendations in the EU Directive 2010/63 for the Care and Use of Laboratory Animals. All animal protocols were approved by the Committee on the Ethics of Animal Experiments of the University of Naples Federico II and the Italian Minister of Health. Every effort was made to minimize animal pain and suffering.

2.2 | Mitochondria isolation and detection of respiration rate

Immediately after excision, fragments of iBAT were deprived of all visible white adipose tissue contaminations, and immersed in ice-cold isolation buffer [220 mM mannitol, 70 mM sucrose, 20 mM Tris-HCl, 1 mM EDTA, 5 mM EGTA, and 1% fatty acid-free bovine serum albumin (BSA), pH 7.4]. Fragments were homogenized in a Potter-Elvehjem homogenizer; the homogenate was then centrifuged at 10 000 *g* for 10 minutes, at 4°C. Floating fat was removed, while the pellet was then re-suspended in the original volume and centrifuged at 500 *g* for 10 minutes; the resulting supernatant was centrifuged at 8000 *g* to obtain a mitochondrial pellet. Mitochondrial pellets were washed twice, re-suspended in a minimal volume of isolation medium, and kept on ice.

Mitochondrial respiration rate was evaluated polarographically using a Clark-type electrode at 30°C. Isolated mitochondria (0.3 mg/mL) were incubated in respiration medium made of 80 mM KCl, 50 mM HEPES (pH 7.0), 1 mM EGTA, 5 mM K_2HPO_4, and 0.5% fatty acid-free BSA (w/v). Respiration was initiated by addition of one of the following substrates: pyruvate (10 mM) + malate (2 mM) or palmitoyl-carnitine (PAL-CAR) (40 μM) + malate (2 mM) or glycerol 3-phosphate (G3P) (6 mM). Progressively, guanosine diphosphate (GDP) (5 mM) and carbonilcyanide *p*-triflouromethoxyphenylhydrazone (FCCP) (2 μM) were added to substrate-energized mitochondria. The presence of EGTA in both the isolation and the respiration buffers allowed us to exclude any variations in the assessed parameters due to putative UCP3-dependent calcium oscillations.

2.3 | Mitochondrial H_2O_2 release and lipid hydroperoxides content

Mitochondria from iBAT of WT and KO mice were assayed in parallel in 96-well plates using a fluorescence microplate reader (Infinite 200 Tecan) set at 37°C, which measured fluorescence of each well every 30 seconds. Mitochondria were suspended at a concentration of 0.1 mg protein/mL in the above-described respiration assay medium, which was previously supplemented with 80 μM Amplex Red, 4 U/mL catalase (CAT), and 2 U/mL horseradish peroxidase (HRP). The reaction was initiated by addition of one of the three substrates: pyruvate (10 mM) + malate (2 mM) or PAL-CAR (40 μM) + malate (2 mM) or G3P (6 mM). HRP catalyzed the reaction between Amplex Red and H_2O_2, in the presence of exogenously added superoxide dismutase (SOD), to form the fluorophore resorufin, with excitation and emission wavelengths at 540 ± 25 nm and 590 ± 25 nm, respectively. H_2O_2 standard curves were generated to calculate the cumulative mitochondrial H_2O_2 production from the resorufin signal at each measurement time-point. The rate of H_2O_2 production was then determined by calculating the rate of change of H_2O_2 concentration over the following 2 minutes, in nmol H_2O_2/min/mg mitochondrial protein. Background rates of fluorescence change in the absence of added substrate were subtracted for each experiment.

Electron leak, representing the percentage of electrons that, during their transport by the respiratory chain, leak from the respiratory chain and reduce oxygen to superoxide, was estimated by dividing the H_2O_2 release (rough index of superoxide production) by the relative respiration rate and by multiplying the results for 100.

Lipid hydroperoxides were determined spectrophotometrically as already reported.[35]

2.4 | Glycerol release from iBAT

Fifty mg of iBAT were used to evaluate the glycerol diffusion from the tissue to the medium; tissues were placed in 250 μL of Krebs Ringer buffer (KRB; 12 mM HEPES, 121 mM NaCl, 4.9 mM KCl, 1.2 mM $MgSO_4$, and 0.33 mM $CaCl_2$) containing 2% FA-free BSA and 0.1% glucose, and incubated in a shaking bath for 1 hour, at 37°C, in the presence of 95% O_2 and 5% CO_2. At the end of the incubation period, an aliquot of the medium was used for the analysis of glycerol. A commercially available absorbance-based enzyme assay for glycerol (Free Glycerol Reagent; Sigma) was converted to fluorescence-based detection by the inclusion of the H_2O_2-sensitive dye Amplex UltraRed, as reported by Clark and coworkers.[36]

2.5 | Overall kinetics of reactions involved in the oxidation of G3P

For the evaluation of the kinetic response of G3P oxidation to a change in mitochondrial membrane potential, mitochondrial respiration rate, and membrane potential were detected in parallel experiments. Mitochondria (0.3 mg/mL) were incubated in the respiration medium supplemented with oligomycin (1 μg/mL) and nigericin (80 ng/mL). Respiration rate was determined as described above in mitochondria energized with G3P as substrate (6 mM), in the absence and in the presence of 2 mM GDP. For membrane potential detection, WT and KO mice mitochondrial membrane potential were assayed in parallel in 96-well plates using a fluorescence microplate reader using the positively charged dye safranin O, which changes fluorescence in a manner linearly proportional to the mitochondrial membrane potential.[37] The safranin O signal for each condition was measured at excitation and emission wavelengths of 540 ± 25 nm and 590 ± 25 nm, respectively, either in absence of G3P, in the presence of G3P (6 mM), and in the presence of G3P (6 mM) plus GDP (2 mM). The relative decrease in fluorescent signal upon energization of the mitochondria was proportional to the membrane potential; results were reported as the absolute magnitude of this change in fluorescence, with larger changes in relative fluorescence units indicating higher membrane potentials.

2.6 | Western blot

To obtain total tissue lysates, iBAT fragments (100 mg) were homogenized in 400 μL of RIPA buffer (150 mM NaCl, 1.0% Triton X-100, 0.5% sodium deoxycholate, 0.1% SDS, 50 mM Tris, and pH 8.0) supplemented with a broad-range antiprotease cocktail (Sigma-Aldrich). Homogenates were left on ice for 1 hour, and then, centrifuged at 17 000 *g* for 30 minutes, at 4°C; the resulting supernatants were collected.

To obtain mitochondrial lysates, mitochondria were isolated as described above with the isolation medium being supplemented with the antiprotease cocktail (Sigma-Aldrich). Isolated mitochondria were diluted in RIPA buffer left on ice for 1 hour, and then, centrifuged at 17 000 *g* for 30 minutes, at 4°C. The obtained supernatants containing lysates without debris were collected. Protein concentration values were determined using the Bio-Rad's DC method (Bio-Rad Laboratories, Hercules, CA); samples were handled in order to obtain protein concentration values of about 4 mg/mL. Primary antibodies used throughout the study were the following: anti-UCP1 (AB1426; Millipore), anti-mitochondrial glycerol-3-phosphate dehydrogenase (mG3PDH) (ab 188585 abcam), anti-SOD-2 (ab 13533; abcam), anti-glutathione peroxidase 4 (GPX-4) (MAB5457 R&D system), anti-CAT (ab 16731 abcam), a cocktail of antibody used to detect CI-NDUF88, CII-SDHB, CIII-UQCRC2, CIV-MTCO1, and CV-ATP VA subunits (oxophos ab110413, abcam), anti-perilipin-1 (PLIN-1) (ab3526 abcam), and anti-adenine nucleotide transferase 1 (ANT-1) (ab 110322 abcam).

Proteins were detected by a chemiluminescence protein-detection method based on the protocol supplied with a commercially available kit (Millipore) and using the appropriate secondary antibodies. Signals were detected using a ChemiDoc™ XRS (Bio-Rad). Protein representation was quantified by densitometry (QuantityOne, BioRad), and normalized based on loading controls, namely β-actin (A2228, Sigma-Aldrich) or α-tubulin (ab4074, abcam) for tissue lysates, and Ponceau S staining or voltage-dependent anion-selective channel (VDAC) (GTX114187 genetex) for mitochondrial lysates.

2.7 | *In-gel* activity staining

Solubilization of mitochondrial membranes with detergents, blue native PAGE (BN-PAGE), staining, and densitometric quantification of oxidative phosphorylation complexes were performed essentially as already described,[38,39] with minor modifications. Briefly, the mitochondria-containing sediment was suspended in a low-salt buffer (50 mM NaCl, 50 mM imidazole, and pH 7.0) and solved with digitonin (4 g/g mitochondrial protein) for solubilization of respiratory chain supercomplexes. Mitochondrial protein extracts (15 μg/mouse/

lane) were subjected to electrophoretic run (carried out on 4%-13% gradient polyacrylamide gels), and immediately after, the enzymatic colorimetric reactions were performed essentially as reported by others.[40,41] Activity staining of mG3PDH was determined by incubating the gel slices with 5 mM Tris-HCl (pH 7.4), 3 mM $MgCl_2$, 0.88 mM menadione, 1.2 mM nitroblue tetrazolium (NTB), 1.5 μM rotenone, 2 μM KCN, and 10 mM G3P for 30 minutes-1 hour, at room temperature.[41] Complex I activity was determined by incubating the gel slices with 2 mM Tris-HCl (pH 7.4), 0.1 mg/mL NADH, and 2.5 mg/mL NTB for 5-15 minutes, at room temperature.[40] Complex IV activity was estimated by incubating BN-PAGE gels with 5 mg of 3,3′-diaminobenzidine tetrahydrochloride (DAB) dissolved in 9 mL of phosphate buffer (0.05 M, pH 7.4), containing 20 μg of CAT, 10 mg of cytochrome c, and 750 mg sucrose, for 10-30 minutes, at room temperature.[40] The original color of the reacting bands was preserved by treating gels in an aqueous solution containing 50% v/v methanol, 10% v/v acetic acid, for 15 minutes, and fixing them in 10% v/v acetic acid. In parallel, another electrophoretic run was performed to stain the gels with Coomassie Blue G and to obtain the total band pattern of the respiratory supercomplexes. Electronic images of the gels were acquired by means of a calibrated GS-800 densitometer (BioRad), and analyzed using QuantityOne software (BioRad). The areas of the bands were expressed as arbitrary units.

2.8 | Two-dimensional (2D) BN-SDS-PAGE and protein identification by mass spectrometry (MS) analysis

After mono-dimensional BN-PAGE, native gel lanes were cut, equilibrated in 1% w/v SDS, and subsequently horizontally laid on the top of 2D-SDS-PAGE 16% T gel for the second dimension separation.[42] Resulting protein spots were visualized by standard ammonia silver staining. Spots from the second dimension were excised, *in-gel* alkylated with iodoacetamide, and digested with trypsin as previously reported.[43] Peptide mixtures were desalted by μZipTipC18 tips (Millipore) prior to nano-liquid chromatography (nanoLC)-electrospray ionization (ESI)-linear ion trap (LIT)-tandem (MS/MS) mass spectrometry (nanoLC-ESI-LIT-MS/MS) analysis, which was performed on a LTQ XL mass spectrometer equipped with UltiMate 3000 HPLC RSLC nanosystem (Thermo Fischer Scientific, USA). Peptides were separated on an Easy C18 column (100 × 0.075 mm, 3 μm), at a flow rate of 300 nL/minutes, using a gradient elution with acetonitrile containing 0.1% formic acid in 0.1% formic acid, as already reported.[44] Mass spectra were acquired in the range *m/z* 400-1400 and data-dependent automatic MS/MS acquisition was applied to the three most abundant ions, enabling dynamic exclusion with repeat count 1 and exclusion duration 60 secconds. Mass isolation window and collision energy for peptide fragmentations were set to *m/z* 3 and 35%, respectively. Raw data from nanoLC-ESI-LIT-MS/MS analysis were searched by MASCOT v2.6.1 (Matrix Science, UK) against a UniProtKB repository with *Mus musculus* taxonomy filter (17147 sequences, 10/2017). The following parameters were used for protein identification: mass tolerance values of 1.8 and 0.8 Da for precursor and fragment ions, respectively; trypsin as proteolytic enzyme with maximum missed-cleavage sites of 2; Cys carbamidomethylation as fixed modification, Met oxidation, and Gln → PyroGlu formation as variable modifications. Protein candidates with at least two significantly matched peptide sequences (expectation value < .05) with ion score > 30 were further considered for definitive protein assignment after manual spectra visualization and verification.

2.9 | Immunoassay for 8-hydroxy-2′-deoxyguanosine (8-OHdG)

A competitive ELISA of 8-OHdG was performed using a DNA/RNA Oxidative Damage ELISA kit (Cayman Chemical Company, Ann Arbor, Michigan, USA) according to the manufacturer's protocol. Serum samples were analyzed in duplicate. Standards of 8-OHdG were assayed over a concentration range of 10.3-3000 pg/mL.

2.10 | Histological analysis and electron microscopy

For histological analysis, samples of iBAT were fixed by immersion in 4% v/v formaldehyde in 0.1 M phosphate buffer at 4°C, overnight. The samples were dehydrated in ethanol, cleared, and embedded in paraffin blocks. The tissues were cut into serial 6-μm-thick sections and stained with hematoxylin-eosin for morphological examination. Sections were viewed with a Nikon Eclipse 80i light microscope (Nikon Instruments, Milan, Italy) at 20× magnification. Images were obtained with a Sony DS-5M camera connected to an ACT-2U image analyzer.

For transmission electron microscopy (TEM), iBAT tissues were dissected and small fragments measuring about 1 mm^3 were fixed in 2% glutaraldehyde, 2% formaldehyde in 0.1 M PBS, pH 7.4, at 4°C, overnight. The specimens were washed with phosphate buffer and post-fixed in 1% osmium tetroxide for 60 minutes, at 4°C; they were then dehydrated in acetone and embedded in an Epon-Araldite mixture. Semithin sections (2 μm) were stained with toluidine blue. Thin sections were obtained with a MTX ultramicrotome (RMC, Tucson, AZ, USA), stained with lead citrate and examined

with a CM10 transmission electron microscope (Philips, Eindhoven, the Netherlands).

2.11 | Statistical analysis

Data were normally distributed and reported as mean ± SEM. Data were analyzed by a two-tailed Student's t test using Graphpad Prism 5 software (Graphpad, San Diego, CA, USA). Differences have been considered statistically significant at $P < .05$.

3 | RESULTS

3.1 | Effect of the absence of UCP3 on the contribution of tissues to body weight, and BAT morphology

The contribution of liver, heart, gastrocnemius, and iBAT to whole animal weight was similar in WT and KO mice, while that of the visceral white adipose tissue resulted reduced in KO mice (Table 1).

Histological analysis showed that iBAT parenchyma of both WT and KO mice acclimated to 22°C was composed of typical multilocular cells. As expected, at thermoneutrality (30°C), brown fat adipocytes acquired a unilocular phenotype in both experimental groups, typical for nonactive tissue. Notably, the effect was less evident in KO mice, both in cells and lipid droplets (LD) size (Figure 1).

3.2 | Absence of UCP3 impacts mitochondrial morphology

High-resolution examining of resin-embedded specimens revealed a nonhomogeneous cytoplasmic staining of BAT parenchyma in KO mice. In this group, some but distinct clusters of adipocytes showed a curiously pale cytoplasm, when the semi-thin sections were stained with toluidine blue (Figure 2A). Ultrastructural analysis of the iBAT from WT mice, performed by TEM, confirmed the unilocular rearrangement of lipid content but also revealed the abundance and the compactness of brown-like mitochondria. These latter were large, numerous, and characterized by a complete double membrane structure, suggesting the typical features of functional mitochondria (Figure 2B,C). Conversely, iBAT from KO mice showed that the weakly stained brown adipocytes revealed extensive signs of mitochondrial degeneration, such as incomplete or complete lack of cristae. The paleness of the cytoplasm derived from the degeneration of the mitochondrial convolutions lacking the inner membrane and the reduction of mitochondria area of intact cristae.

3.3 | Absence of UCP3 impacts iBAT glycerol release and PLIN-1 protein abundance

To test whether the altered LD morphology observed in iBAT of KO mice acclimated at thermoneutrality should be associated with an enhanced lipolysis, we detected tissue glycerol release (ie, a functional marker of lipolysis) as well as PLIN-1 protein levels, in view of the role played by such a protein in protecting lipid droplet by the attach of lipases. As reported in Figure 3, glycerol release was significantly enhanced (+45%) in KO mice, with respect to WT (Figure 3A), while PLIN-1 tissue levels were significantly reduced (−65%) in the same comparison (Figure 3B).

3.4 | Absence of UCP3 does not affect neither tissue mitochondrial content nor UCP1 protein levels

We next examined if the absence of UCP3 affected UCP1 protein levels, given the crucial importance of this component in influencing BAT thermogenesis and physiology. In order to evaluate whether iBAT mitochondrial content should differ between UCP3 KO and WT mice, we determined: (a) the mitochondrial protein recovery from 100 mg of tissue, (b) the representation levels of an inner mitochondrial membrane protein marker, namely adenine nucleotide translocase (ANT-1). Mitochondrial recovery was independent of the genotype, being 3.5 ± 0.2 and 3.4 ± 0.3 mg mitochondrial protein/g tissue in WT and KO mice, respectively. Furthermore, no differences in protein content of ANT-1 were detected between

TABLE 1 Body weight and organ weights in WT and KO mice

	Body weight	Liver	Heart	Gastrocnemius	iBAT	vWAT
	(g)	(g tissue/g animal) 100				
WT	22 ± 0.5	4.87 ± 0.19	0.53 ± 0.02	1.14 ± 0.04	0.82 ± 0.09	3.75 ± 0.47
KO	21 ± 0.3	4.37 ± 0.27	0.57 ± 0.03	1.2 ± 0.06	0.63 ± 0.06	2.42 ± 0.3*

Note: Values represent the mean ± SE (n = 8).

*$P < .05$ vs WT.

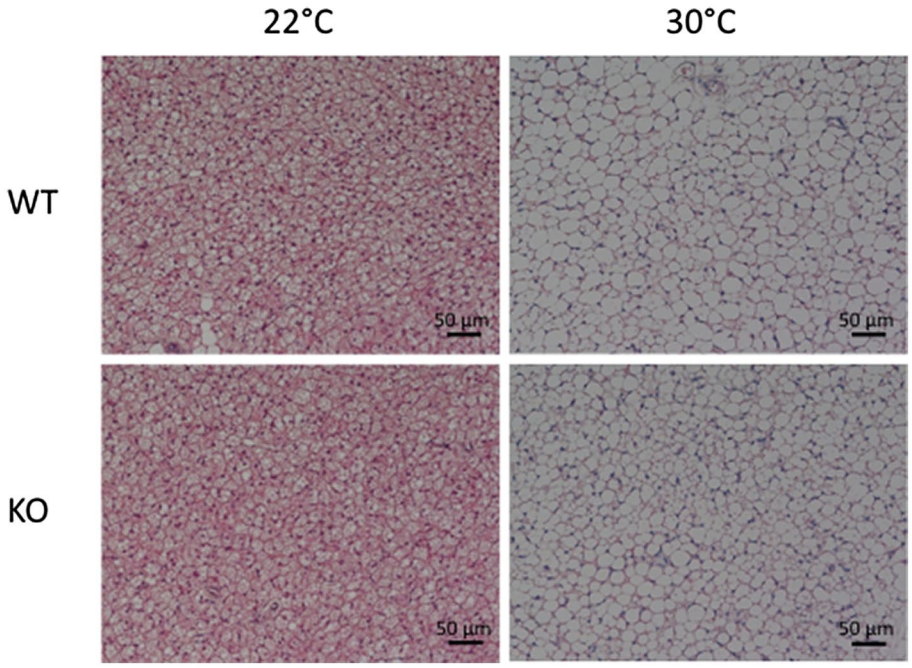

FIGURE 1 Histological analysis of iBAT from WT and KO mice. Representative histological analysis of iBAT from WT and KO mice acclimated at standard temperature (22°C) and at thermoneutrality (30°C) since weaning. Hematoxylin and eosin staining

WT and KO mice, either when its levels were detected in total tissue and in isolated mitochondrial lysates (Figure 4). Collectively, these data indicated that iBATs from WT and KO mice have similar mitochondrial content.

No differences in UCP1 protein levels were observed between WT and KO mice, when this protein was assayed in lysates from isolated mitochondria or from total tissues (Figure 5).

3.5 | The absence of UCP3 influences palmitoyl-carnitine oxidation rate and the overall activity of the reactions involved in the oxidation of G3P in isolated iBAT mitochondria

The ablation of UCP3 affects iBAT mitochondrial oxygen consumption, depending on the respiratory substrate. When using pyruvate (+ malate), no significant differences in basal respiration rate were detected between WT and KO mice (Figure 6A). GDP addition to the mitochondrial incubation induced a genotype-independent decrease in respiration rate of about 30%. The subsequent addition of FCCP induced an increase in the respiration rate, which reached levels higher than those observed under basal conditions, indicating a proper mitochondrial quality (Figure 6A). When using palmitoyl-carnitine (+ malate) as substrate, a significant lower respiration rate was observed in mitochondria from KO mice (−25%) vs WT littermates (Figure 6B). GDP added to respiration medium induced a decrease in respiration rate both in WT and KO mice, but oxygen consumption remained lower in KO mice (Figure 6B).

In the presence of G3P, mitochondria from KO mice showed a reduced respiration rate (−60%), when compared to WT littermates. A similar reduction was observed in the presence of GDP as well as of FCCP (Figure 6C), suggesting that alterations in the reactions involved in the oxidation of G3P take place in KO mice. This possibility was sustained by the evidence that the overall kinetics of G3P oxidation were inhibited in iBAT mitochondria from KO compared to WT littermates, since at any given membrane potential, mitochondria from WT mice showed higher respiration rates (Figure 7).

Experiments concerning the overall activity of the reactions involved in the oxidation of specific substrates were restricted to G3P; thus, indication on those involved in oxidation of pyruvate was limited to data obtained on oxygen consumption in the presence of FCCP that, as reported above, was not affected by the absence of UCP3.

Western blot analysis revealed similar levels of mG3PDH and of the five mitochondrial respiratory complexes in iBAT mitochondria from WT and KO mice (Figure 8).

We next evaluated if the absence of UCP3 may affect the activity of mG3PDH or respiratory Complexes I and IV. To this aim, iBAT mitochondria were solubilized with the mild detergent digitonin; resulting proteins were resolved by BN-PAGE and subsequently assayed for *in-gel* activities (Figure 9). mG3PDH resulted to be present in several homo-oligomers (presumably trimer, tetramer) as well as in high molecular mass supercomplexes (SC) (Figure 9A).

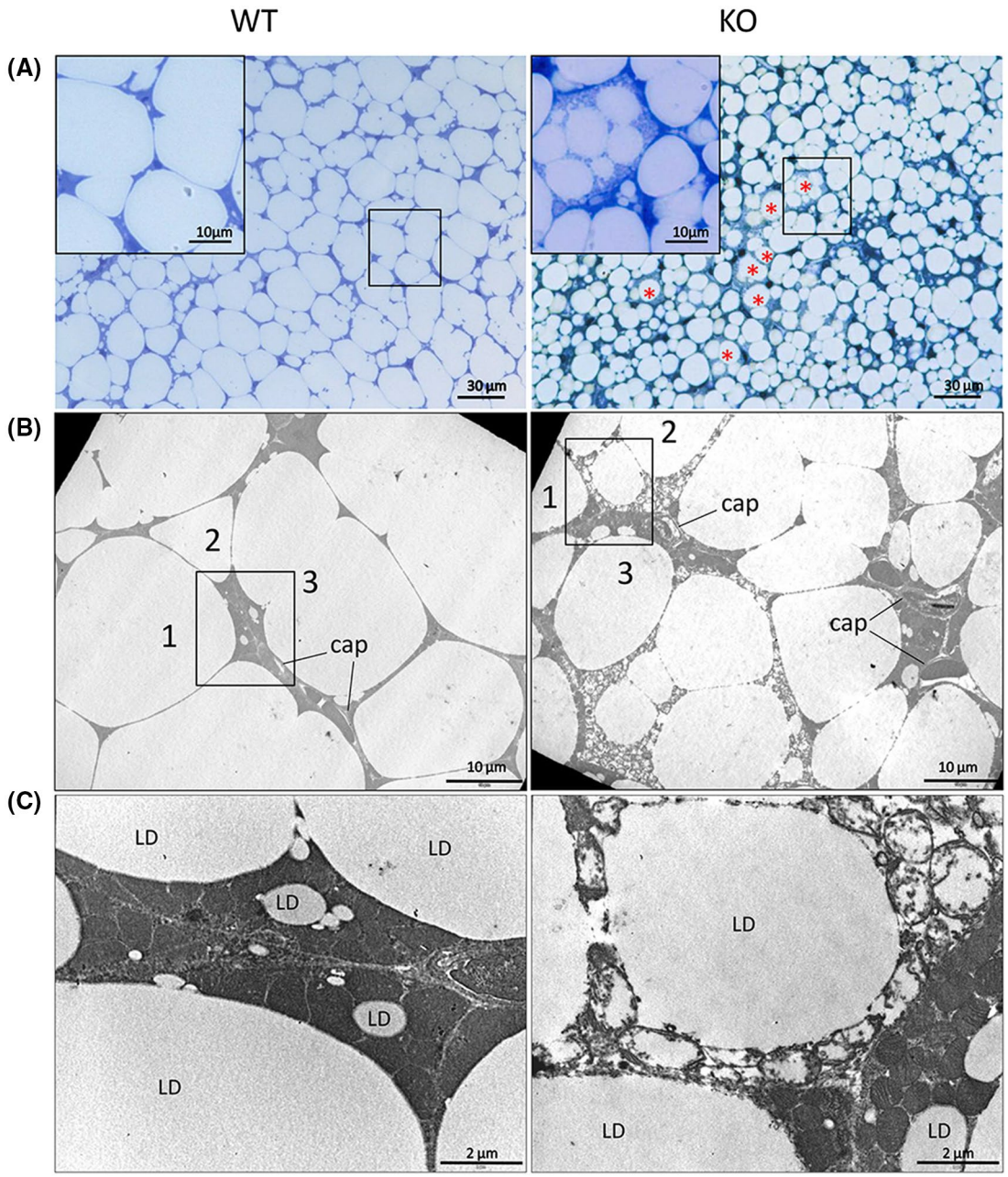

FIGURE 2 Electron microscopy analysis of iBAT from WT and KO mice. Light micrographs (A) and electron micrographs (B and C) of iBAT parenchyma from WT and KO mice, acclimated at thermoneutrality (30°C) since weaning. A, Large LD and an uniformly blue-stained cytoplasm characterized the typical warm-acclimated brown adipocyte from WT mice. iBAT from KO mice showed smaller LD than those found in WT mice and a nonhomogeneous cytoplasmic staining. Some weakly blue - stained multilocular adipocytes were detected (panel A, red asterisk and inset). Resin embedding, toluidine blue stained. B, The low magnification electron micrograph of the framed areas in panel A revealed both the electron dense cytoplasmic rim of the adipocytes from WT mice and the fine ultrastructure of the pale adipocytes (as shown in panel A, *left*), exhibiting a clear cytoplasm containing many membrane-bound structures such as mitochondria. C, The high magnification of the framed area in B showed the corresponding mitochondrial shape of three adjacent adipocytes (named 1, 2, 3), respectively, from both WT and KO mice. Numerous, large mitochondria with intact cristae (complete inner membrane) were found in the adipose cells from WT mice. The clear cytoplasmic rim of the pale adipose cell, detected in KO mice parenchyma, revealed densely packed mitochondria with obvious signs of degeneration, such as incomplete or complete lack of internal mitochondrial membrane. No signs of mitochondrial degeneration were shown in the mitochondria of the closely apposed cells. cap, capillary. Scale bar: A = 30 µm, insets = 10 µm; B = 10 µm; C = 2 µm

However, mG3PDH activity was prominent within the mass range 146/720, with the band at about 250 kDa, presumably the holoenzyme, showing the highest activity (Figure 9A). Interestingly, in some heavier SCs, mG3PDH activity coexisted with Complex I and/or Complex IV activities (co-migration of mG3PDH with subunits of Complex I and

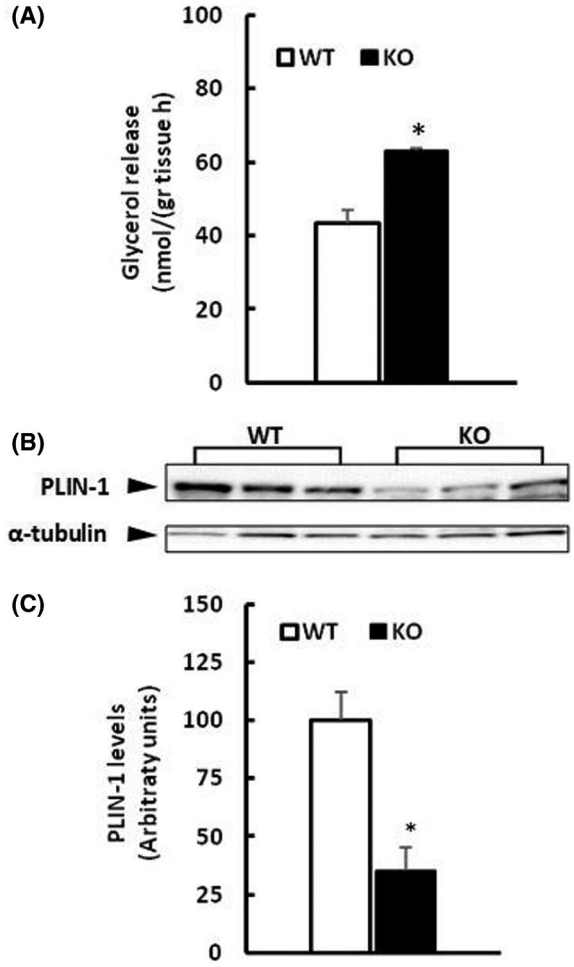

FIGURE 3 Glycerol release and PLIN-1 protein abundance in iBAT from WT and KO mice. Data on glycerol release and PLIN-1 protein abundance are reported in panels A, B, and C, respectively. Panel B shows a representative Western blot of PLIN-1 levels detected in iBAT tissue lysates (15 μg of protein/mouse/lane) from WT and KO mice. C, Histograms represent quantification of Western blot data. Data were normalized to the value obtained for WT animals, set as 100. Values represent the mean ± SE of six different mice. *$P < .01$ vs WT

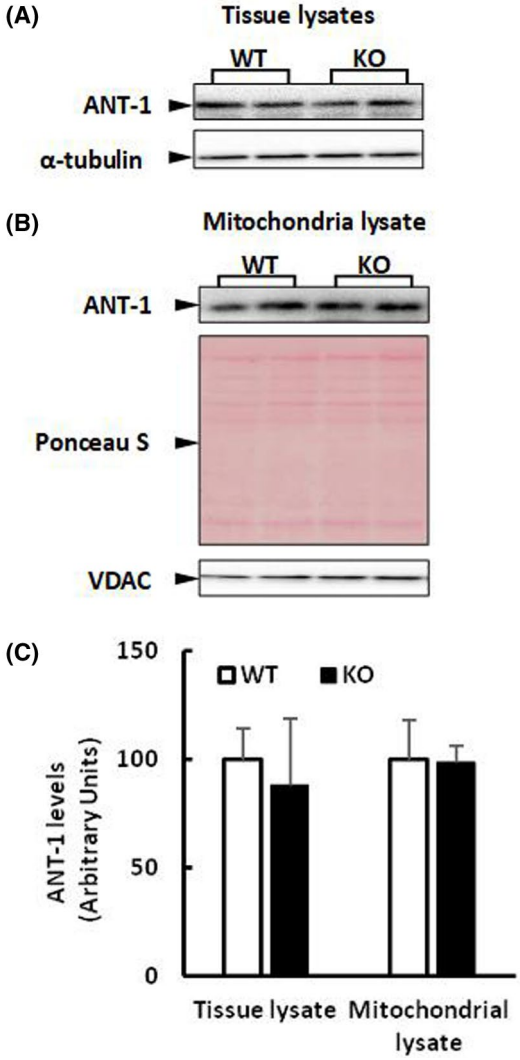

FIGURE 4 ANT-1 representation levels in iBAT from WT and KO mice. Representative Western blots of ANT-1 levels detected in tissue (A) and mitochondrial (B) lysates of iBAT from WT and KO mice. α-tubulin, and Ponceau S or VDAC were used as loading controls for total tissue lysates (15 μg of protein/mouse/lane) and mitochondrial lysates (15 μg of protein/mouse/lane), respectively. C, Histograms represent quantification of data; "mitochondrial lysate" refers to normalization on Ponceau S. Data were normalized to the value obtained for WT animals, set as 100. Values represent the mean ± SE of six different mice

Complex IV in mono-dimensional BN-PAGE was corroborated by subsequent 2D BN-SDS-PAGE, see Supporting Data 1 and 2). Densitometric analysis revealed that the absence of UCP3 was associated with a significant reduction of the *in-gel* activity of mG3PDH detected in all the three most intense colored bands (migrating at 250, 418, and 540 kDa) (Figure 9D).

Two respiratory complex-derived bands that corresponded to SCs with apparent molecular mass values of 935 and 824 kDa revealed Complex I (NADH-dehydrogenase) activity (Figure 9B). Four bands, corresponding to SCs with apparent molecular weights of 824, 730, 614, and 418 kDa, showed Complex IV activity (Figure 9C). No significant differences in the *in-gel* activities between WT and KO mice were observed, neither for Complex I nor for Complex IV (Figure 9E,F).

3.6 | Absence of UCP3 enhances mitochondrial oxidative stress and activates enzymatic antioxidant defenses

We next tested if the absence of UCP3 could have affected mitochondrial H_2O_2 release as well as electron leak, that is,

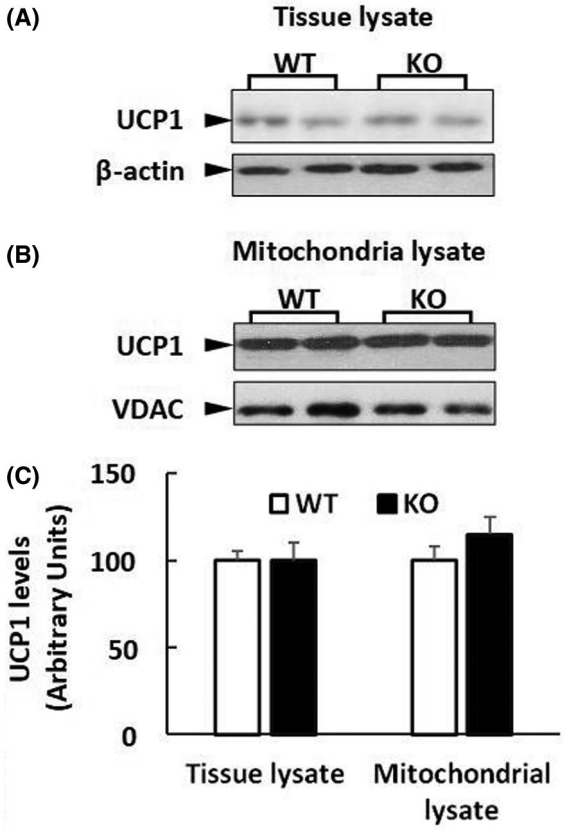

FIGURE 5 UCP1 representation levels in iBAT from WT and KO mice. Representative Western blots of UCP1 levels detected in tissue (A) and mitochondrial (B) lysates of iBAT from WT and KO mice. β-actin and VDAC were used as loading controls for total tissue lysates (15 μg of protein/mouse/lane) and mitochondrial lysates (15 μg of protein/mouse/lane), respectively. C, Histograms represent quantification of data. Data were normalized to the value obtained for WT animals, set as 100. Values represent the mean ± SE of six different mice

the percentage of electrons that, during their transport by the respiratory chain, leak from the latter, and reduce oxygen to superoxide. Regardless of the used substrate, no significant changes in H_2O_2 release were observed between WT and KO mice (Figure 10A); moreover, when using G3P as substrate, electron leak was significantly enhanced in KO mice (Figure 10B).

Moreover, mitochondria lacking UCP3 showed a strong increase in the levels of the antioxidant enzymes SOD-2, CAT, and GPX4 (Figure 11). Despite their enhanced antioxidant defense profile, the same mitochondria, when compared to those of WT mice, had increased lipid hydroperoxides, which is an index of oxidative damage to lipids (Figure 10C). An enhanced oxidative stress in absence of UCP3 was also detected in the periphery, since sera of KO mice showed higher levels of 8-OHdG (a critical biomarker of oxidative stress) compared to those observed in WT counterparts (+50% vs WT) (Figure 10D). Since we used whole body UCP3 KO mice, it should be emphasized that the observed increase in serum 8-OHdG may be a consequence of augmented oxidative stress in other UCP3-expressing tissues.

3.7 | Absence of UCP3 influences mitochondrial protein assembly in respiratory SCs

The Coomassie blue-stained electrophoretic profiles of SCs obtained for iBAT mitochondria from WT and KO mice after digitonin extraction and subsequent mono-dimensional BN-PAGE are shown in Figure 10A and 10B, respectively. Densitometric analysis revealed that iBAT mitochondria from WT mice contained two protein bands, within the range 730-830 kDa (arrows in Figure 12A), which were more faint in KO mice (−30% and −50% vs WT, for the heavier and the lighter one, respectively, with a statistic significance at $P < .05$). To isolate and identify protein subunits present in these bands, native gel lanes were cut and subsequently run on 2D SDS-PAGE gels (Figure 12C,D). Protein spots of interest (numbered in Figure 12C) were excised, digested with trypsin, and subjected to nanoLC-ESI-LIT-MS/MS. Table 2 lists the detected proteins. Each of the analyzed spots resulted to be a miscellaneous of co-migrating proteins, among which components of the fatty acid oxidation machinery, that is, trifunctional enzyme, very long-specific acyl-CoA dehydrogenase, acyl-CoA dehydrogenase, propionyl-CoA carboxylase, and enoyl-CoA isomerase, proteins involved in the maintenance of the mitochondria shape and cristae organization, that is, subunits of the MICOS complex and of F1F0-ATP synthase (complex V), and subunits of complexes I and III. mG3PDH was also detected (for details, see Supporting Data 1 and 2).

4 | DISCUSSION

The role of UCP3 in BAT remains enigmatic due to the high abundance of UCP1. Here, we report data suggesting that the absence of UCP3 in mice housed at thermoneutrality has a significant impact on BAT oxidative metabolism, enhances mitochondrial oxidative stress, and alters mitochondrial structure in some adipocytes, with UCP1 being normally expressed.

The absence of UCP3 lowered the ability of BAT mitochondria to use specific metabolic respiratory substrates, such as G3P and palmitoyl-carnitine. Concerning G3P oxidation, this pathway involves mG3PDH, a ubiquinone-linked flavoprotein localized at the outer side of the mitochondrial inner membrane that, by oxidizing "cytosolic/glycolytic"-produced NADH, converts G3P into dihydroxyacetone

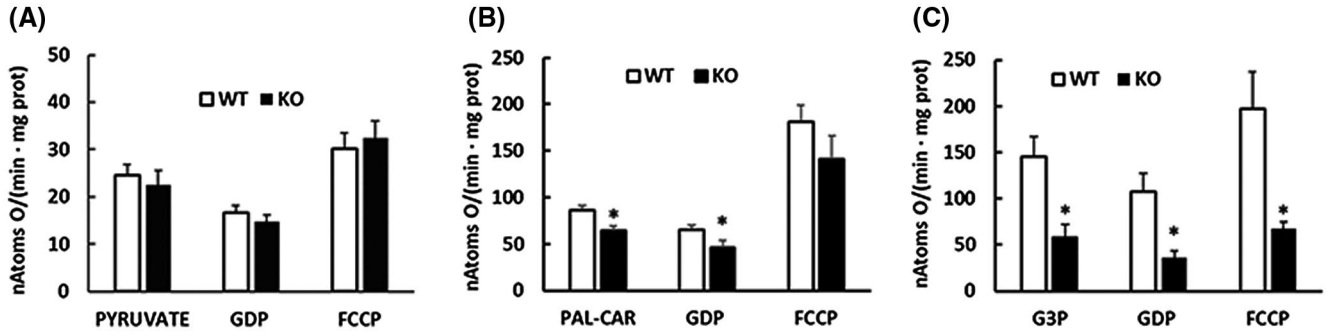

FIGURE 6 Respiration rate of iBAT mitochondria from WT and KO mice Mitochondria were incubated in respiration medium at a concentration of 0.3 mg/mL and were energized with different substrates: pyruvate (+ malate) (A), palmitoyl-carnitine (PAL-CAR) (+malate) (B) and glycerol-3-phosphate (G3P) (C). Respiration were detected in the basal condition and in the presence of GDP and FCCP sequentially added to the respiration medium. Values represent the mean ± SE of five measurements in the case of pyruvate + malate and of nine different measurements when the other substrates were used. *$P < .05$ vs WT

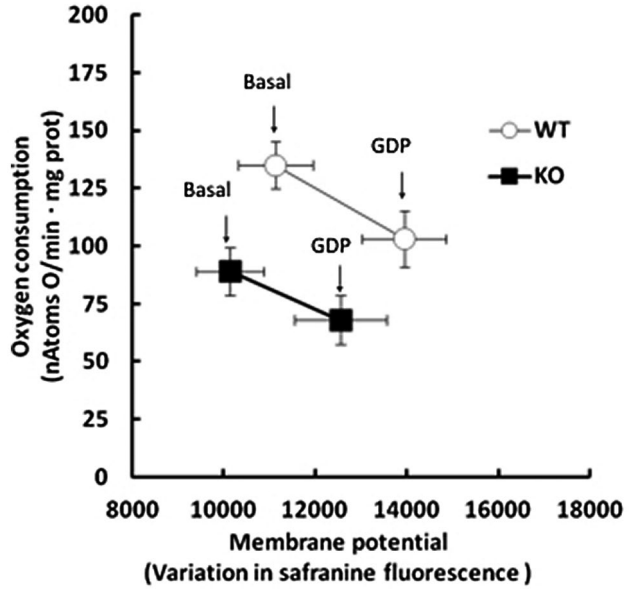

FIGURE 7 Overall activity of reactions involved in the oxidation of G3P in iBAT mitochondria from WT and KO mice. Mitochondria were incubated in respiration medium at a concentration of 0.3 mg/mL; for each group, membrane potential and mitochondrial respiration were detected in parallel experiments in mitochondria energized with G3P in the absence and in the presence of GDP. Values represent the mean ± SE of eight different measurements

phosphate, with concurrent reduction of FAD to $FADH_2$, and transfers the electrons to Complex III through coenzyme Q (CoQ). Physiologically, this process has two important consequences: (a) it allows a high rate of cytosolic ATP production, very important in brown adipocytes, because of the low mitochondrial ATP production; (b) it contributes to reduce mitochondria efficiency, since the oxidation of NADH via G3P shuttle is non-efficient, when compared to NADH oxidation via Complex I.[45] These phenomena could have been both affected in BAT of KO mice, producing functional alterations.

Since the protein levels of mG3PDH and of other respiratory complexes were unaffected by the absence of UCP3, the reduced oxidation of G3P, and the lower mG3PDH *in-gel* activity observed in KO mice may have been due to post-translational mechanisms involving the enzyme. Several factors are known to allosterically modulate mG3PDH; among these, worth mentioning are Ca^{2+}, which activates the enzyme, and oxidative stress and lipid metabolites (such free fatty acids and acyl-CoAs) that inhibit it.[46-48] The higher lipolytic capacity of iBAT of KO mice associated with the lower ability of mitochondria to use lipid derived substrates, such as palmitoyl-carnitine, allowed us to speculate that acyl-CoAs may accumulate at the mitochondrial level, thus inhibiting mG3PDH.

Concerning Ca^{2+}, data from the literature indicate that UCP3 is associated with calcium handling[49,50] and that UCP3 depletion in Hela cells strongly reduces the cytosolic and the mitochondrial Ca^{2+} elevations evoked by histamine.[49] In the present study, it is unlike that modifications in calcium handling in brown adipocyte of KO mice could have contributed to the observed impaired ability of mitochondria to oxidize G3P or to the lower *in-gel* activity of G3PDH, since: (a) calcium chelators were present both in the mitochondrial isolation medium and in the respiration medium; and (b) the measurement of the *in-gel* activity of G3PDH was performed in the absence of Ca^{2+}.

Additionally, it has been reported that mG3PDH can associate into homo-oligomers as well as into higher molecular weight SCs, which represent native forms of the enzyme in the membrane.[42] Alterations in such mG3PDH-containing supramolecular structures might also be involved in the observed effects. Generally, the supramolecular organization of respiratory chain components is functional to improve the electron transport rate and to limit/balance ROS generation.[51] We observed that the BN-PAGE profile of digitonin-extracted mitochondrial proteins from WT mice presented at least two bands that were over-represented,

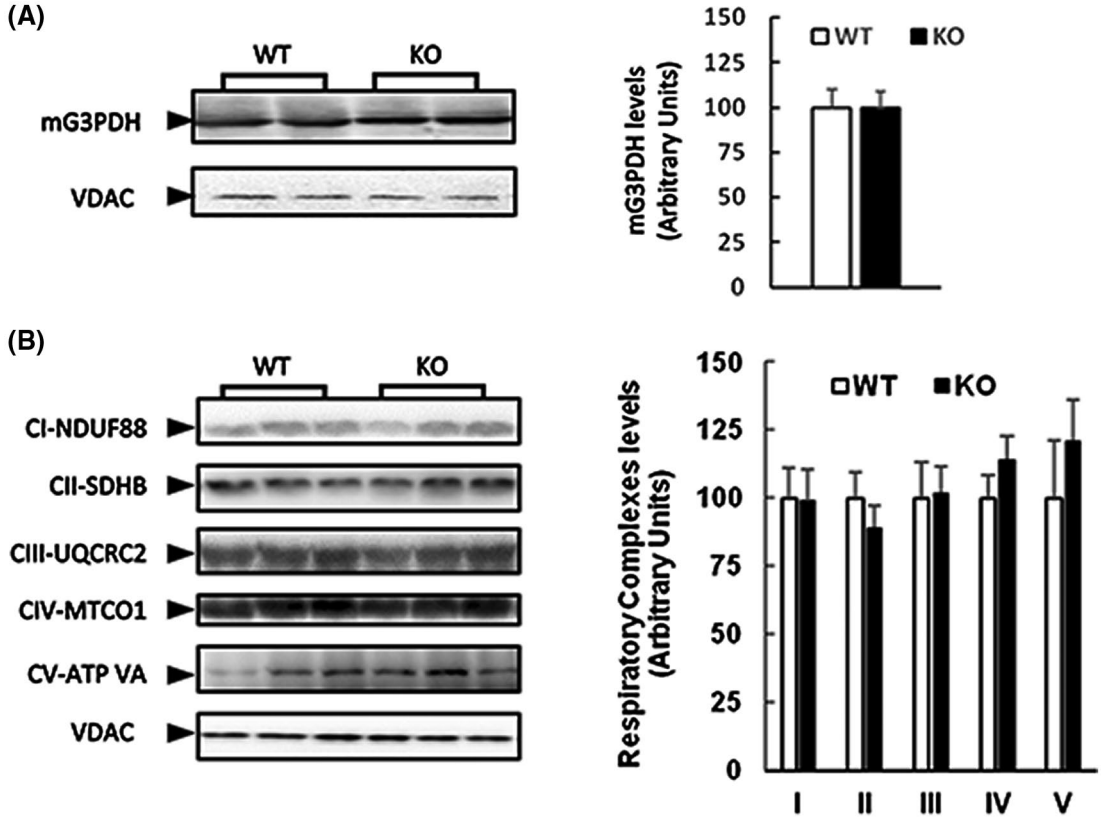

FIGURE 8 mG3PDH and respiratory complexes abundance in iBAT mitochondria from WT and KO mice. Representative Western blots of mG3PDH (A) as well as of CI-NDUF88, CII-SDHB, CIII-UQCRC2, CIV-MTCO1, and CV-ATP VA subunits (B) in isolated mitochondria from iBAT of WT and KO mice (15 μg of protein/mouse/lane). Histograms represent quantification of data. Data were normalized to the value obtained for WT animals, set as 100. Values represent the mean ± SE of 7/8 different mice

when compared to KO counterparts, thus indicating that the absence of UCP3 can modify the assembly or the levels of specific protein complexes. 2D BN-SDS-PAGE combined with nanoLC-ESI-LIT-MS/MS analysis allowed us to identify some proteins present in the multi-enzymatic complexes over-represented in WT mice, and their assignment to a functional context. Identified proteins, even in miscellaneous, included among the others mG3PDH and Complex III, thus suggesting that G3PDH and Complex III does not properly assemble in mitochondria from KO mice or not assemble at all.

Interestingly, it should be considered that mG3PDH is also an important site of superoxide production,[41,52-55] and, in BAT, it seems to be responsible for about 63% of the total H_2O_2 production.[55] The impaired assembly of mG3PDH in KO mice could also underlie the higher percentage of electrons that, during their transport by respiratory chain, leak from the respiratory chain, and reduce oxygen to $O_2^{\bullet-}$. In line with this consideration, our data indicate that *the first line defense antioxidants*, which are strategic to protect mitochondria from the damage induced by $O_2^{\bullet-}$, including mitochondrial SOD-2, CAT, and GPX-4, was significantly enhanced in KO mice. This suggests the occurrence of compensatory mechanisms in mitochondria lacking UCP3, which are likely finalized to remove $O_2^{\bullet-}$ and to metabolize H_2O_2 as well as lipid hydroperoxides. Despite the huge increase in the above antioxidant enzymes, the release in H_2O_2 (resulting from the balance of its production and metabolism) seemed not affected by the absence of UCP3, thus indicating a likely higher ability of BAT mitochondria of KO mice to produce ROS. This was supported by the evidences that in mitochondria from KO mice: (a) a higher electron leak took place (see also above); and (b) increased oxidative damage of mitochondrial lipids were observed. Enhanced oxidative damage associated with the absence of UCP3 would also contribute to the systemic oxidative stress evident in sera of KO mice. Since we used whole body ablated-UCP3 mice, other tissues expressing UCP3, such as skeletal muscle or heart, could have contributed to the observed systemic oxidative stress.

As cited above, our data indicate that BAT mitochondria from KO mice displayed a reduced ability to oxidize palmitoyl-carnitine. In BAT, β-oxidation of fatty acids is important not only for cold-induced activation[56] but also at thermoneutrality for the maintenance of the tissue functionality.[57] Our data are also in line with what observed in mitochondria from skeletal muscle of KO mice,[28,29,58] and with the evidence that UCP3 abundance correlates with the degree of fatty acid oxidation.[30] From a molecular point of

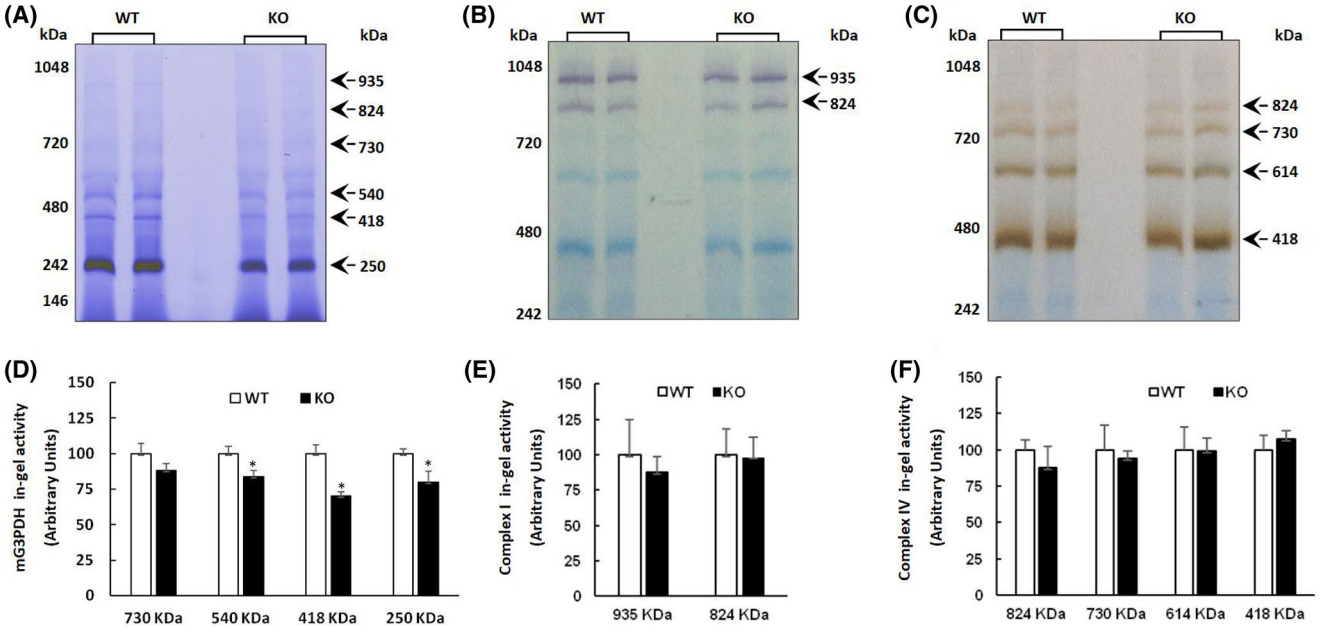

FIGURE 9 BN-PAGE-based analysis of *in-gel* activity of mG3PDH, Complexes I and IV in digitonin-solubilized crude mitochondria from iBAT of WT and KO mice. Panels show representative images of histochemical staining of mG3PDH- (A), Complex I- (B), and Complex IV- (C) *in-gel* activities. Molecular mass of standard proteins (on the left) and the relative position of the respiratory SCs are indicated (arrows). D-F, Densitometric quantification of the colored bands corresponding to *in-gel* activity of the indicated SCs. Data were normalized to the value obtained for WT animals, set as 100. Values represent the mean ± SE of three different mice. $*P < .05$ vs WT

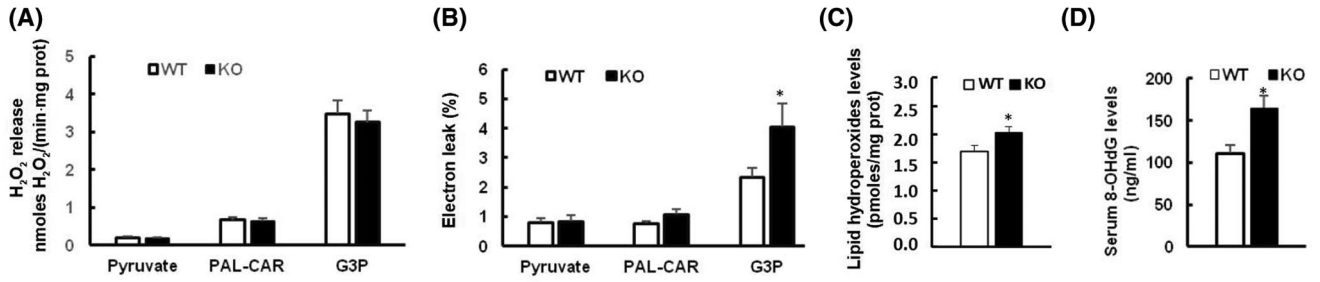

FIGURE 10 H_2O_2 release (A), electron leak (B), and lipid hydroperoxides (C) levels detected in iBAT mitochondria from WT and KO mice. D, 8-OHdG levels detected in serum of WT and KO mice. In panel A and B, mitochondria were energized with different substrates: pyruvate (+ malate), palmitoyl-carnitine (PAL-CAR) (+malate), or glycerol-3-phosphate (G3P). In panel B, electron leak represents the percentage of electrons that, during their transport by the respiratory chain, leak from the respiratory chain and reduce oxygen to superoxide. For each substrate, electron leak has been evaluated by dividing mitochondrial H_2O_2 release (expressed in nmoles H_2O_2/min mg prot) for the relative mitochondrial oxygen consumption (expressed in nmoles O_2/min mg proteins), and by multiplying it for 100. Values represent the mean ± SE of six different measurements, in the case of H_2O_2 release and electron leak, and of eight different measurements, in the case of lipid hydroperoxides and 8-OHdG levels. $*P < .05$ vs WT

view, it should be considered that the enzymes involved in β-oxidation of fatty acids carry out their function in the context of a multienzyme complex. Our data, concerning the analysis of the proteins present in those multi-complexes over-represented in WT mice, identified also enzymes involved in fatty acid oxidation. Thus, the alteration in their levels/supramolecular aggregation could indeed contribute to the reduced ability of KO mitochondria to use fatty acids as metabolic substrates.

Other proteins identified in the present paper, as occurring in the multi-complexes over-represented in WT mice, included components involved in the formation and stabilization of cristae junction structures (eg, MICOS) as well as subunits of F1F0-ATP synthase. In particular, MICOS establishes contact sites between the inner and outer mitochondrial membranes, and its deficiency leads to a grossly altered inner membrane architecture and disorganized cristae.[59] The cristae shape is also governed by F1F0-ATP-synthase dimers,[60]

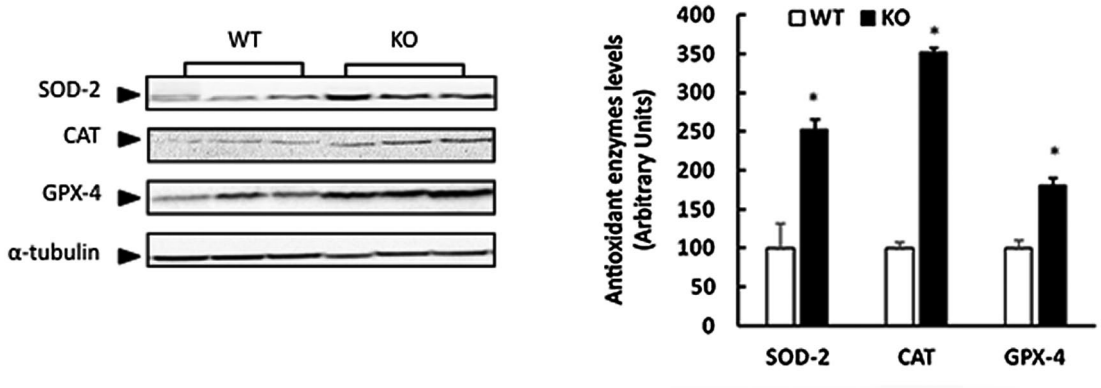

FIGURE 11 Abundance of mitochondrial antioxidant enzymes in iBAT from WT and KO mice. Representative Western blots of superoxide dismutase 2 (SOD-2), catalase (CAT), and glutathione peroxidase 4 (GPX-4) in iBAT lysate (15 μg of protein/mouse/lane). Histograms represent quantification of data. Data were normalized to the value obtained for WT animals, set as 100, and represent the mean ± SE of four different mice. *$P < .01$ vs WT

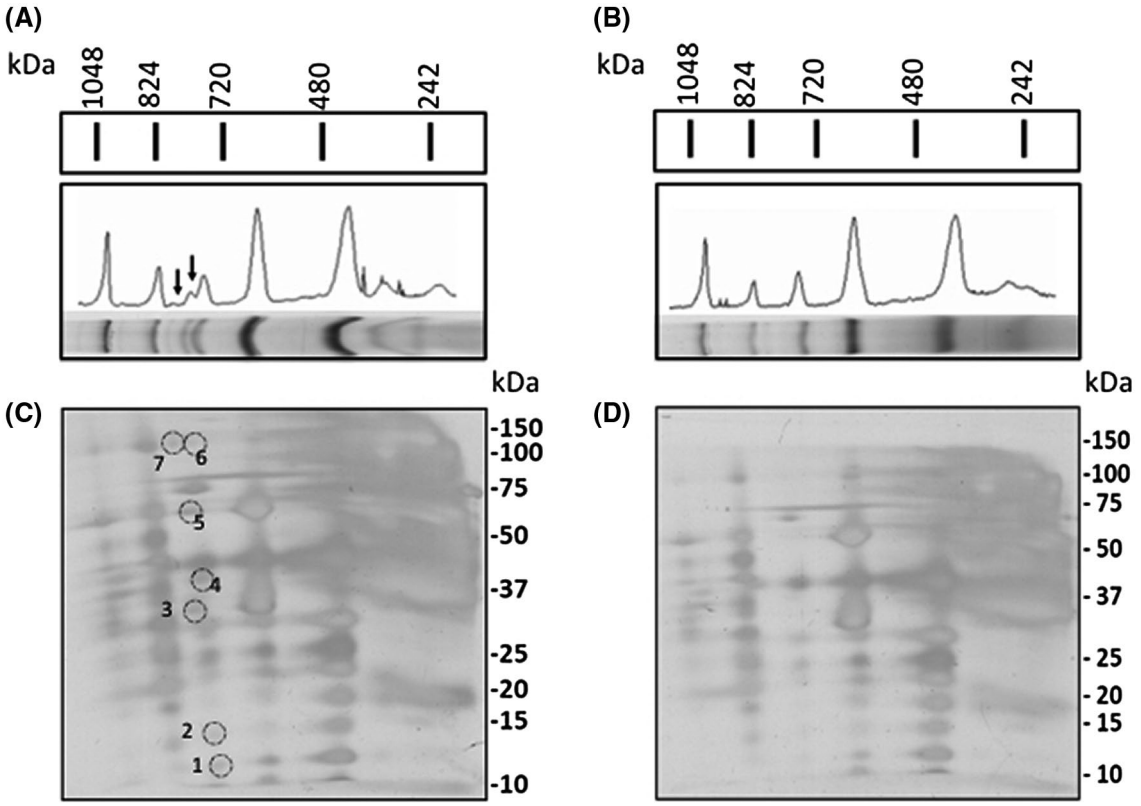

FIGURE 12 2D-BN-SDS-PAGE-based analysis of mitochondrial SC in iBAT from WT and KO mice. Mono-dimensional BN-PAGE-based analysis of digitonin-solubilized crude mitochondria from BAT of WT (A) and KO (B) mice. Representative images of Coomassie blue-stained BN-PAGE lanes are reported. Bands characteristic of OXPHOS SCs are recognizable. Representative density traces for OXPHOS SC bands are also showed. Arrows in (A) indicate protein bands detected in WT but significantly fainter in KO mice. On the top, the positions of standard proteins for molecular mass are also indicated. Native gel slices were subsequently horizontally laid on the top of 16% T 2D-SDS-PAGE gels, which were subjected to separation and obtained spots were visualized by silver staining (C and D). Protein identification of selected spots was based on analysis performed as previously reported.[40,41] For identification details, see Supporting Data 2

which are linked together back-to-face by DAPIT (diabetes-associated protein in insulin-sensitive tissue), forming long oligomers along the edges of the cristae.[61] Several subunits of the F1F0-ATP synthase as well as DIAPIT were found in the spots specifically present in mitochondria of WT mice and down-represented in KO ones. Results were in good accordance with the inadequate cristae organization and shape observed in mitochondria localized in some

TABLE 2 Differentially represented proteins in 2D BN-SDS-PAGE maps of iBAT mitochondria from WT and KO mice in the mass range 730-830 kDa grouped for their functions in respiratory chain, fatty acid oxidation, and mitochondrial and cristae shape.

Spot	Respiratory chain	Fatty acid oxidation	Mitochondrial and cristae shape
1	Cytochrome c oxidase subunit 6C Cytochrome b-c1 complex Rieske		
2	ATP synthase subunit e ATP synthase subunit g ATP synthase subunit f Cytochrome b-c1 complex subunit 8		ATP synthase subunit e ATP synthase subunit g ATP synthase subunit f
3	ATP synthase F(0) complex subunit B1 ATP synthase subunit alpha Cytochrome c1 NADH dehydrogenase [ubiquinone] 1 beta subcomplex subunit 10 NADH dehydrogenase [ubiquinone] iron-sulfur protein 3 Cytochrome b-c1 complex subunit 2 Cytochrome b-c1 complex subunit Rieske		MICOS complex subunit Mic19 MICOS complex subunit Mic27 ATP synthase F(0) complex subunit B1 ATP synthase subunit alpha
4	ATP synthase subunit alpha ATP synthase subunit gamma		ATP synthase subunit alpha ATP synthase subunit gamma
5	ATP synthase subunit beta NADH dehydrogenase [ubiquinone] iron-sulfur protein 2 Cytochrome b-c1 complex subunit 1 Cytochrome b-c1 complex subunit 2	Trifunctional enzyme subunit beta Alpha-enolase Propionyl-CoA carboxylase alpha chain	MICOS complex subunit Mic60
6	ATP synthase subunit alpha ATP synthase subunit beta Glycerol-3-phosphate dehydrogenase Cytochrome b-c1 complex subunit 1 Cytochrome b-c1 complex subunit 2	Acyl-CoA dehydrogenase family member 9 Very long-chain specific acyl-CoA dehydrogenase Trifunctional enzyme subunit alpha Fatty acid synthase Propionyl-CoA carboxylase alpha chain Propionyl-CoA carboxylase beta chain	ATP synthase subunit alpha ATP synthase subunit beta
7	ATP synthase subunit alpha ATP synthase subunit beta Cytochrome b-c1 complex subunit 1 Cytochrome b-c1 complex subunit 2 Glycerol-3-phosphate dehydrogenase	Very long-chain specific acyl-CoA dehydrogenase Trifunctional enzyme subunit alpha Trifunctional enzyme subunit beta Fatty acid synthase -CoA carboxylase beta chain Propionyl-CoA carboxylase alpha chain Propionyl subunit 2	MICOS complex subunit Mic60

Note: Mitochondrial iBAT proteins were extracted, separated by 2D BN-SDS-PAGE, and identified by nanoLC-ESI-LIT-MS/MS following *in-gel* digestion with trypsin. Spot numbering refers to Figure 12C, Supporting Data 1 and 2.

but distinct subsets of brown adipocytes from KO mice. Specifically, these mitochondria appeared swollen with decreased electron density within the matrix, the cristae being thinner, mis-oriented, and/or disassembled. Interestingly, the adipocytes containing such altered mitochondria were surrounded by others with normal mitochondrial morphology. This is a very intriguing aspect, together with the fact that brown adipocytes from KO mice appeared to have smaller LDs and more multilocular lipid droplets; the latter condition in these cells is generally associated with an increased mitochondrial activity and an increased fat oxidation (such us during cold exposure), rather than a reduced mitochondrial activity. Despite detailed and focused experiments are needed to address these points, at a speculative level, it is possible to suggest that in cells in which the antioxidant capacity is not able to adequately contrast the oxidative stress, mitochondrial degeneration, observable at the morphological level, takes place. Furthermore, the observed signs of mitochondrial alteration could be the "starting point" of an age-dependent degenerative tissue process, likely at the begin in the young animals we used in this study.

Concerning the relation between LD morphology and mitochondrial activity, the observed discrepancy could be more apparent than real, since the deposition of TG and the

formation of LD are processes that require ATP and the absence of UCP3, by negatively influencing mitochondrial G3P oxidation, likely slows cytosolic energy production, which is crucial for the brown adipocyte's biology (see also above). In addition, the smaller LD observed in BAT of mice lacking UCP3 could be explained by an enhanced lipolysis, since a higher glycerol release and the reduction in PLIN-1 protein levels were observed in KO mice. Indeed, PLIN1 is a key protein that restricts adipose lipolysis under basal condition, by reducing the access of cytosolic lipases to triacylglycerol substrates stored in the lipid droplets.[62] The increase in lipolysis associated with the absence of UCP3 in KO mice is not limited to BAT, since it also occurs in white adipose tissue (29, and data not shown). Future studies will reveal the molecular mechanisms underlying the enhanced lipolysis in adipose tissues associated with the absence of UCP3.

Data here reported indicate a clear impact of the absence of UCP3 on mitochondrial functionality in mice housed at thermoneutrality, and lead open the question if this is an issue of adaptation to the lower need for thermogenesis at 30°C, or if the effect is also evident when mice are housed at standard temperature. We were not able to show a difference in G3P-supported respiration rate when mice were housed at 22°C (data not shown); this suggested that chronic housing of mice under conditions of thermal stress as standard temperature (22°C) might mask the genetic functions involved in energy balance and metabolic homeostasis. This concept was previously addressed by original studies on UCP1-ablated mice,[6] and this is also the case of UCP3 KO mice. Indeed, while Gong and coworkers[13] failed to show a reduced metabolic rate in KO mice housed at 22°C vs their WT control, we did at thermoneutrality.[29] Whether or not the metabolic adaptations induced at thermoneutrality in iBAT from UCP3 KO mice can be recapitulated by re-activation of thermogenesis, for example, by a hypercaloric diet feeding, is a very interesting still open question. Another important issue has to be emphasized; since we did not use a BAT specific UCP3-KO mice, rather we employed whole body UCP3 KO mice, we cannot exclude that factors released by other tissues expressing UCP3 could have contributed to influence BAT functionality in our model. Further studies employing BAT-specific UCP3 KO mice will help to clarify this aspect.

As a whole, the results of the present paper indicate that, at thermoneutrality, the lack of UCP3 exerts detrimental effects on both BAT functionality and the supramolecular organization of mitochondrial proteins that, in turn, is crucial for: (a) preserving adequate substrate oxidation rate; (b) limiting the oxidative stress; and (c) ensuring the proper assembly of mitochondrial cristae.

CONFLICT OF INTEREST

The authors declare no conflict of interest.

AUTHOR CONTRIBUTIONS

E. Silvestri and R. Senese performed research, analyzed data, wrote, and revised the paper; R. De Matteis, F. Cioffi, A. Gentile, and RA Busiello performed research and analyzed data; AM Salzano and A. Scaloni performed research, analyzed data, and revised the paper; M. Moreno, A. Lanni, P. de Lange, and F. Goglia designed research and revised the paper; A. Lombardi designed research, analyzed data, wrote, and revised the paper.

REFERENCES

1. Cannon B, Nedergaard J. Brown adipose tissue: function and physiological significance. *Physiol Rev*. 2004;84(1):277-359.
2. Bartelt A, Bruns OT, Reimer R, et al. Brown adipose tissue activity controls triglyceride clearance. *Nat Med*. 2011;17(2):200-205. https://doi.org/10.1038/nm.2297
3. van Marken Lichtenbelt WD, Vanhommerig JW, Smulders NM, et al. Cold-activated brown adipose tissue in healthy men. *N Engl J Med*. 2009;360(15):1500-1508. Erratum. In: N Engl J Med. 2009 360(18):1917. https://doi.org/10.1056/NEJMoa0808718
4. Nedergaard J, Bengtsson T, Cannon B. New powers of brown fat: fighting the metabolic syndrome. *Cell Metab*. 2011;13(3):238-240. https://doi.org/10.1016/j.cmet.2011.02.009
5. Boss O, Farmer SR. Recruitment of brown adipose tissue as a therapy for obesity-associated diseases. *Front Endocrinol (Lausanne)*. 2012;3:14. https://doi.org/10.3389/fendo.2012.00014
6. Feldmann HM, Golozoubova V, Cannon B, Nedergaard J. UCP1 ablation induces obesity and abolishes diet-induced thermogenesis in mice exempt from thermal stress by living at thermoneutrality. *Cell Metab*. 2009;9(2):203-209. https://doi.org/10.1016/j.cmet.2008.12.014
7. Masand R, Paulo E, Wu D, et al. Proteome imbalance of mitochondrial electron transport chain in brown adipocytes leads to metabolic benefits. *Cell Metab*. 2018;27(3):616-629.e4. https://doi.org/10.1016/j.cmet.2018.01.018
8. Reitman ML. Of mice and men - environmental temperature, body temperature, and treatment of obesity. *FEBS Lett*. 2018;592(12):2098-2107. https://doi.org/10.1002/1873-3468.13070
9. Hilse KE, Kalinovich AV, Rupprecht A, et al. The expression of UCP3 directly correlates to UCP1 abundance in brown adipose tissue. *Biochim Biophys Acta*. 2016;1857(1):72-78. https://doi.org/10.1016/j.bbabio.2015.10.011
10. Pohl EE, Rupprecht A, Macher G, Hilse KE. Important trends in UCP3 Investigation. *Front Physiol*. 2019;10:470. https://doi.org/10.3389/fphys.2019.00470
11. de Lange P, Lanni A, Beneduce L, et al. Uncoupling protein-3 is a molecular determinant for the regulation of resting metabolic rate by thyroid hormone. *Endocrinology*. 2001;142(8):3414-3420.
12. Enerbäck S, Jacobsson A, Simpson EM, et al. Mice lacking mitochondrial uncoupling protein are cold-sensitive but not obese. *Nature*. 1997;387(6628):90-94.
13. Gong DW, Monemdjou S, Gavrilova O, et al. Lack of obesity and normal response to fasting and thyroid hormone in mice lacking uncoupling protein-3. *J Biol Chem*. 2000;275(21):16251-16257.
14. Mills EM, Banks ML, Sprague JE, Finkel T. Pharmacology: uncoupling the agony from ecstasy. *Nature*. 2003;426(6965):403-404.
15. Mills EM, Rusyniak DE, Sprague JE. The role of the sympathetic nervous system and uncoupling proteins in the thermogenesis

induced by 3,4-methylenedioxymethamphetamine. *J Mol Med (Berl)*. 2004;82(12):787-799.
16. Riley CL, Dao C, Kenaston MA, et al. The complementary and divergent roles of uncoupling proteins 1 and 3 in thermoregulation. *J Physiol*. 2016;594(24):7455-7464. https://doi.org/10.1113/JP272971
17. Sprague JE, Mallett NM, Rusyniak DE, Mills E. UCP3 and thyroid hormone involvement in methamphetamine-induced hyperthermia. *Biochem Pharmacol*. 2004;68(7):1339-1343.
18. Nau K, Fromme T, Meyer CW, von Praun C, Heldmaier G, Klingenspor M. Brown adipose tissue specific lack of uncoupling protein 3 is associated with impaired cold tolerance and reduced transcript levels of metabolic genes. *J Comp Physiol B*. 2008;178(3):269-277.
19. Ozcan C, Palmeri M, Horvath TL, Russell KS, Russell RR 3rd. Role of uncoupling protein 3 in ischemia-reperfusion injury, arrhythmias, and preconditioning. *Am J Physiol Heart Circ Physiol*. 2013;304(9):H1192-H1200. https://doi.org/10.1152/ajpheart.00592.2012
20. Perrino C, Schiattarella GG, Sannino A, et al. Genetic deletion of uncoupling protein 3 exaggerates apoptotic cell death in the ischemic heart leading to heart failure. *J Am Heart Assoc*. 2013;2(3):e000086. https://doi.org/10.1161/JAHA.113.000086
21. Cadenas S. Mitochondrial uncoupling, ROS generation and cardioprotection. *Biochim Biophys Acta Bioenerg*. 2018;1859(9):940-950. https://doi.org/10.1016/j.bbabio.2018.05.019
22. Busiello RA, Savarese S, Lombardi A. Mitochondrial uncoupling proteins and energy metabolism. *Front Physiol*. 2015;6:36. https://doi.org/10.3389/fphys.2015.00036
23. Schrauwen P, Russell AP, Moonen-Kornips E, Boon N, Hesselink MK. Effect of 2 weeks of endurance training on uncoupling protein 3 content in untrained human subjects. *Acta Physiol Scand*. 2005;183(3):273-280.
24. Schrauwen P, Mensink M, Schaart G, et al. Reduced skeletal muscle uncoupling protein-3 content in prediabetic subjects and type 2 diabetic patients: restoration by rosiglitazone treatment. *J Clin Endocrinol Metab*. 2006;91(4):1520-1525.
25. Echtay KS, Roussel D, St-Pierre J, et al. Superoxide activates mitochondrial uncoupling proteins. *Nature*. 2002;415(6867):96-99.
26. Lombardi A, Busiello RA, Napolitano L, et al. UCP3 translocates lipid hydroperoxide and mediates lipid hydroperoxide-dependent mitochondrial uncoupling. *J Biol Chem*. 2010;285(22):16599-16605. https://doi.org/10.1074/jbc.M110.102699
27. Milloux RJ, Harper ME. Uncoupling proteins and the control of mitochondrial reactive oxygen species production. *Free Radic Biol Med*. 2011;51(6):1106-1115. https://doi.org/10.1016/j.freeradbiomed.2011.06.022
28. Senese R, Valli V, Moreno M, et al. Uncoupling protein 3 expression levels influence insulin sensitivity, fatty acid oxidation, and related signaling pathways. *Pflugers Arch*. 2011;461:153-164. https://doi.org/10.1007/s00424-010-0892-3
29. Lombardi A, Busiello RA, De Matteis R, et al. Absence of uncoupling protein-3 at thermoneutrality impacts lipid handling and energy homeostasis in mice. *Cells*. 2019;8(8):E916. https://doi.org/10.3390/cells8080916
30. Hilse KE, Rupprecht A, Egerbacher M, et al. The expression of uncoupling protein 3 coincides with the fatty acid oxidation type of metabolism in adult murine heart. *Front Physiol*. 2018;9:747. https://doi.org/10.3389/fphys.2018.00747
31. Bloor ID, Symonds ME. Sexual dimorphism in white and brown adipose tissue with obesity and inflammation. *Horm Behav*. 2014;66(1):95-103. https://doi.org/10.1016/j.yhbeh.2014.02.007
32. Choi DK, Oh TS, Choi JW, et al. Gender difference in proteome of brown adipose tissues between male and female rats exposed to a high fat diet. *Cell Physiol Biochem*. 2011;28(5):933-948. https://doi.org/10.1159/000335807
33. Rodriguez-Cuenca S, Pujol E, Justo R, et al. Sex-dependent thermogenesis, differences in mitochondrial morphology and function, and adrenergic response in brown adipose tissue. *J Biol Chem*. 2002;277(45):42958-42963. https://doi.org/10.1074/jbc.M207229200
34. Valle A, García-Palmer FJ, Oliver J, Roca P. Sex differences in brown adipose tissue thermogenic features during caloric restriction. *Cell Physiol Biochem*. 2007;19(1–4):195-204. https://doi.org/10.1159/000099207
35. Heath RL, Tappel AL. A new sensitive assay for the measurement of hydroperoxides. *Anal Biochem*. 1976;76(1):184-191.
36. Clark AM, Sousa KM, Jennings C, MacDougald OA, Kennedy RT. Continuous-flow enzyme assay on a microfluidic chip for monitoring glycerol secretion from cultured adipocytes. *Anal. Chem*. 2009;81(6):2350-2356. https://doi.org/10.1021/ac8026965
37. Akerman KE, Wikstrom MK. Safranine as a probe of the mitochondrial membrane potential. *FEBS Lett*. 1976;68:191-197.
38. Schagger H. Native electrophoresis for isolation of mitochondrial oxidative phosphorylation protein complexes. *Methods Enzymol*. 1995;260:190-202.
39. Lombardi A, Silvestri E, Cioffi F, et al. Defining the transcriptomic and proteomic profiles of rat ageing skeletal muscle by the use of a cDNA array, 2D- and Blue native-PAGE approach. *J Proteomics*. 2009;72(4):708-721.
40. Zerbetto E, Vergani L, Dabbeni-Sala F. Quantification of muscle mitochondrial oxidative phosphorylation enzymes via histochemical staining of blue native polyacrylamide gels. *Electrophoresis*. 1997;18(11):2059-2064.
41. Mráček T, Holzerová E, Drahota Z, et al. ROS generation and multiple forms of mammalian mitochondrial glycerol-3-phosphate dehydrogenase. *Biochim Biophys Acta*. 2014;1837(1):98-111. https://doi.org/10.1016/j.bbabio.2013.08.007
42. Schägger H, Cramer WA, von Jagow G. Analysis of molecular masses and oligomeric states of protein complexes by blue native electrophoresis and isolation of membrane protein complexes by two-dimensional native electrophoresis. *Anal Biochem*. 1994;217(2):220-230.
43. Arioli S, Roncada P, Salzano AM, et al. The relevance of carbon dioxide metabolism in *Streptococcus thermophilus*. *Microbiology*. 2009;155(Pt 6):1953-1965. https://doi.org/10.1099/mic.0.024737-0
44. Salzano AM, Novi G, Arioli S, Corona S, Mora D, Scaloni A. Mono-dimensional blue native-PAGE and bi-dimensional blue native/urea-PAGE or/SDS-PAGE combined with nLC-ESI-LIT-MS/MS unveil membrane protein heteromeric and homomeric complexes in *Streptococcus thermophilus*. *J Proteomics*. 2013;94:240-261. https://doi.org/10.1016/j.jprot.2013.09.007
45. Mráček T, Drahota Z, Houštěk J. The function and the role of the mitochondrial glycerol-3-phosphate dehydrogenase in mammalian tissues. *Biochim Biophys Acta*. 2013;1827(3):401-410. https://doi.org/10.1016/j.bbabio.2012.11.014
46. Garrib A, McMurray WC. Purification and characterization of glycerol-3-phosphate dehydrogenase (flavin-linked) from rat liver mitochondria. *J Biol Chem*. 1986;261(17):8042-8048.
47. Rauchová H, Drahota Z, Rauch P, Fato R, Lenaz G. Coenzyme Q releases the inhibitory effect of free fatty acids on mitochondrial glycerophosphate dehydrogenase. *Acta Biochim Pol*. 2003;50(2):405-413.

48. Bukowiecki LJ, Lindberg O. Control of sn-glycerol 3-phosphate oxidation in brown adipose tissue mitochondria by calcium and acyl-CoA. *Biochim Biophys Acta*. 1974;348(1):115-125.
49. De Marchi U, Castelbou C, Demaurex N. Uncoupling protein 3 (UCP3) modulates the activity of Sarco/endoplasmic reticulum Ca2+-ATPase (SERCA) by decreasing mitochondrial ATP production. *J Biol Chem*. 2011;286(37):32533-32541. https://doi.org/10.1074/jbc.M110.216044
50. Motloch LJ, Gebing T, Reda S, Schwaiger A, Wolny M, Hoppe UC. UCP3 regulates single-channel activity of the cardiac mCa1. *J Menbr Biol*. 2016;249(4):577-584. https://doi.org/10.1007/s00232-016-9913-2
51. Lenaz G, Genova ML. Supramolecular organisation of the mitochondrial respiratory chain: a new challenge for the mechanism and control of oxidative phosphorylation. *Adv Exp Med Biol*. 2012;748:107-144. https://doi.org/10.1007/978-1-4614-3573-0_5
52. Miwa S, Brand MD. Mitochondrial matrix reactive oxygen species production is very sensitive to mild uncoupling. *Biochem Soc Trans*. 2003;31(Pt 6):1300-1301.
53. Miwa S, Brand MD. The topology of superoxide production by complex III and glycerol 3-phosphate dehydrogenase in Drosophila mitochondria. *Biochim Biophys Acta*. 2005;1709(3):214-219.
54. Vrbacký M, Drahota Z, Mrácek T, et al. Respiratory chain components involved in the glycerophosphate dehydrogenase-dependent ROS production by brown adipose tissue mitochondria. *Biochim Biophys Acta*. 2007;1767(7):989-997.
55. Orr AL, Quinlan CL, Perevoshchikova IV, Brand MD. A refined analysis of superoxide production by mitochondrial sn-glycerol 3-phosphate dehydrogenase. *J Biol Chem*. 2012;287(51):42921-42935. https://doi.org/10.1074/jbc.M112.397828
56. Calderon-Dominguez M, Mir JF, Fucho R, Weber M, Serra D, Herrero L. Fatty acid metabolism and the basis of brown adipose tissue function. *Adipocyte*. 2015;5(2):98-118. https://doi.org/10.1080/21623945.2015.1122857
57. Gonzalez-Hurtado E, Lee J, Choi J, Wolfgang MJ. Fatty acid oxidation is required for active and quiescent brown adipose tissue maintenance and thermogenic programing. *Mol Metab*. 2018;7:45-56. https://doi.org/10.1016/j.molmet.2017.11.004
58. McBride S, Wei-LaPierre L, McMurray F, et al. Skeletal muscle mitoflashes, pH, and the role of uncoupling protein-3. *Arch Biochem Biophys*. 2019;663:239-248. https://doi.org/10.1016/j.abb.2019.01.018
59. Friedman JR, Mourier A, Yamada J, McCaffery JM, Nunnari J. MICOS coordinates with respiratory complexes and lipids to establish mitochondrial inner membrane architecture. *Elife*. 2015;4:e07739. https://doi.org/10.7554/eLife.07739
60. Quintana-Cabrera R, Mehrotra A, Rigoni G, Soriano ME. Who and how in the regulation of mitochondrial cristae shape and function. *Biochem Biophys Res Commun*. 2018;500(1):94-101. https://doi.org/10.1016/j.bbrc.2017.04.088
61. He J, Ford HC, Carroll J, et al. Assembly of the membrane domain of ATP synthase in human mitochondria. *Proc Natl Acad Sci U S A*. 2018;115(12):2988-2993. https://doi.org/10.1073/pnas.1722086115
62. Sztalryda C, Brasaemle DL. The perilipin family of lipid droplet proteins: Gatekeepers of intracellular lipolysis. *Biochim Biophys Acta Mol Cell Biol Lipids*. 2017;1862(10):1221-1232. https://doi.org/10.1016/j.bbalip.2017.07.009.

SUPPORTING INFORMATION

Additional supporting information may be found online in the Supporting Information section.

How to cite this article: Silvestri E, Senese R, De Matteis R, et al. Absence of uncoupling protein 3 at thermoneutrality influences brown adipose tissue mitochondrial functionality in mice. *The FASEB Journal*. 2020;34:15146–15163. https://doi.org/10.1096/fj.202000995R